SAND2022-1070C

ASTFE American Society of Thermal and Fluids Engineers

7th Thermal and Fluids Engineering Conference (TFEC)
April - May, 2022
Partially Online Virtual and in Las Vegas, NV Conference

TFEC-2022-40932

Validating a Fire Simulation Tool with a Large-scale Helium Plume Dataset

Alexander L. Brown, John C. Hewson

Sandia National Laboratories, Albuquerque, NM 87185, USA

ABSTRACT

Fires of practical interest are often large in scale and involve turbulent behavior. Fire simulation tools are often utilized in an under-resolved prediction to assess fire behavior. Data are scarce for large fires because they are difficult to instrument. A helium plume scenario has been used as a surrogate for much of the fire phenomenology (O'Hern et al., 2005), including buoyancy, mixing, and advection. A clean dataset of this nature makes an excellent platform for assessing model accuracy. We have been participating in a community effort to validate fire simulation tools, and the SIERRA/Fuego code is compared here with the historical dataset. Our predictions span a wide range of length-scales, and comparisons are made to species mass fraction and two velocity components for a number of heights in the core of the plume. We detail our approach to the comparisons, which involves some accommodation for the uncertainty in the inflow boundary condition from the test. We show evolving improvement in simulation accuracy with increasing mesh resolution and benchmark the accuracy through comparisons with the data.

KEY WORDS: Helium, Plumes, CFD, Validation

1. INTRODUCTION

The fire science community has been participating in a workshop series known as Measurement and Computation of Fire Phenomena (MaCFP) that is aimed at identifying and promoting solutions to accuracy and quality assurance problems for fire modeling tools. A working group involves participants from around the globe and has focused on simulating a series of high-quality tests. The first two workshops included comparisons to a large-scale helium plume dataset. (https://github.com/MaCFP/macfp-db) [1].

In the interest of validating buoyant turbulent mixing for fire codes, a test campaign was conducted at Sandia's FLAME facility (O'Hern et al., 2005) [2]. A 1-m diameter diffuser was located part way up in the facility to introduce helium into otherwise calm air. A shroud around the diffuser mimicked a ground condition. A light flow was induced from below to allow the plume to draw air and simulate a semi-infinite condition. The test involved planar laser induced fluorescence (PLIF) for species concentrations, and particle image velocimetry (PIV) for velocities. The plume was ostensibly axi-symmetric, though the test was conducted in a rectangular enclosure. The test resulted in a plane of data for velocity and concentration that includes temporal statistics as well as mean vector and scalar quantities. The data were primarily reported in the 1-m region directly above the diffuser. While the plane suggested some degree of symmetry, it was not perfect, and represents an uncertainty in the system.

The facility was well characterized for flow accuracy prior to testing. Pitot and hot wire velocity probes were used to scan over the flow surfaces to characterize the uniformity of the inflow boundaries. Boundaries consisted of honeycomb flow channels that induce a pressure drop across the inflow surface and helped to

*Corresponding Author: albrown@sandia.gov

eliminate any pressure and/or eddy effects in the inflow conditions. The historical reports may be examined for further details on the accuracy of the test conditions (Blanchat, 2001) [3].

The particular case of the helium plume lacks certain complicating physics of interest to fire modeling. It is missing radiation, reactions, soot, and the rest of the physics that accompany these phenomena. It is a good problem for validation because it includes much of what is important. It is fully turbulent (≈1 m source characteristic scale) with density gradients and mixing. It is also amenable to optical diagnostics, as the plume is transparent. The diagnostics were able to illuminate a center-plane with a laser sheet and detect with reasonable accuracy and signal-to-noise the behavior of the plume. This included particle image velocimetry (PIV) and planar laser induced fluorescence (PLIF) measurements for velocity and concentration. While this is not the perfect dataset for fire model validation, it is one of the better ones because it is of relevant scale, has high-quality data, and provides relatively high levels of detail for quality model comparisons.

This paper leverages the MaCFP-produced simulations from SIERRA/Fuego and performs quantitative analysis comparing the data and models. The methods followed herein permit an improved understanding of the effect of mesh resolution on the accuracy of buoyant plume mixing and transport models.

2. METHODS

This study involves comparisons between SIERRA/Fuego and the measured data from O'Hern et al. (2005) [1]. The 1-meter diameter diffuser sourced the helium into the domain where a plane of PLIF provided a measure concentration, and PIV provided a measure of velocity. The primary parameter of study with the simulation tool is the mesh resolution. There are a number of parameters of uncertainty with respect to modeling tools, some of which are not part of the present study. All material properties have uncertainty, and there are geometric uncertainties including non-symmetric and small variations that are neglected in this effort. The mesh resolution was selected as a key parameter for study due to the points outlined in the prior section. Added resolution is increasingly able to resolve the instabilities, which is suspected of lending to some of the larger inaccuracies of the modeling. The role of this is important to fire modeling efforts. Fire models are often used in under-resolved conditions, and it is significant to benchmark the effect on accuracy of the use of an under-resolved prediction to model a complex flow problem.

3.1 Simulation Tool

SIERRA/Fuego is a low-Mach reacting flow module in the Thermal/Fluids suite of simulation tools. The code was designed with a focus on being able to predict the heat transfer to objects in fires. This effort used Version 4.54.2 for all simulations. A user manual and a theory manual are both available publications detailing the specifics of the computational fluid dynamics (CFD) theory and implementation [4-5]. The code is massively parallel and uses a variety of unstructured elements. A differentiating factor in SIERRA/Fuego is that the code is finite-element based instead of a more traditional control volume formulation. A control volume finite element formulation (CVFEM) is used to access some of the more traditional features of a control-volume-based model.

A variety of models are available for most of the physics relevant for a fire prediction, allowing a model form assessment with each prediction. In this particular case, the KSGS large eddy simulation (LES) formulation was used, with light upwinding (factor 0.02) and no under-relaxation. The conservation equations are solved in a segregated manner sequentially with an outer non-linear loop to ensure consistency among the conservation equations. The non-linear iteration was cycled 5 times within a timestep to allow for convergence of the solution within each timestep. The mixture state was modeled using a mixture fraction model and constitutive models for the air and helium streams were formulated from a thermodynamics database using a mixture rule for non-binary mixtures. The mixture fraction is linear in the composition varying from air to the helium source with unity Lewis numbers (the ratio of the thermal to mass diffusivity) assumed. The unity Lewis number assumption is not generally appropriate for helium-air mixtures, but in fully turbulent flows differential diffusion effects tend to be small (Kerstein, A.R., M.A. Cremer, and P.A. McMurtry, 1995) [6].

Simulations were run for eight seconds to allow the initial conditions to develop towards steady state, after which the Favre averaged parameters were accumulated for another 15 seconds. This averaging process repeated, and for the coarsest cases a second 15 second average was obtained and observed to be adequately similar to the first. Puffing frequency was about 1.4 Hz, which means 20+ cycles contributed to the averages.

2.2 Geometry

Figure 1 (left) shows an image with modified dimensions for a subsequent test to the tests performed following the helium plume effort. The facility and stand are all consistent with the helium plume tests. The top of the pedestal and the lack of a circular shroud are the differences between this geometry figure and the geometry of the tests. The documentation of the tests should be consulted for the best description of configuration. The z direction is always vertical, and the radial direction is either x or y (interchangeable due to symmetry).

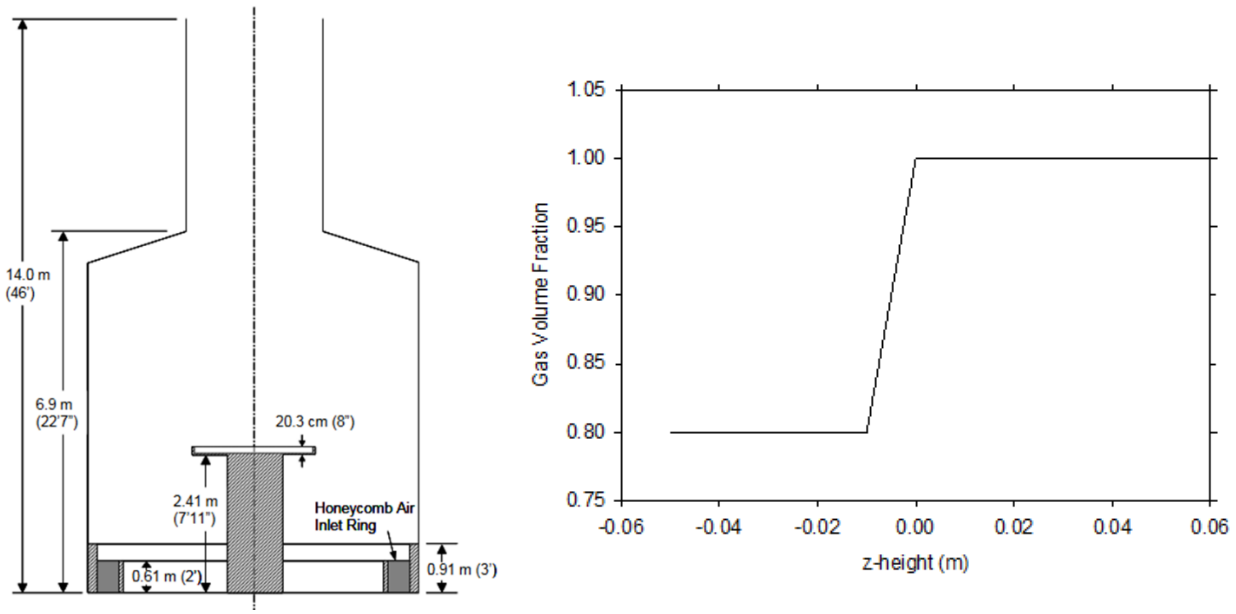

Fig. 1 An illustration of the FLAME facility configured for a pool fire test (left) with the gas volume fraction applied to the inlet condition (right)

2.3 Diffuser Model

The inlet condition was difficult to model for a CFD code. The diffuser consisted of a honeycomb layer with a total thickness of 10.2 cm and 0.3 cm cells at the interface with the domain. The experimental assumption was that the diffuser would create a pressure drop and reduce or eliminate the influence of the domain behavior on the inflow boundary condition. In reality, this assumption is difficult to verify. To model this condition in the simulations, a porous region was assigned below the level of the honeycomb to induce a pressure drop. The flow was allowed to penetrate into the diffuser, but the porous model would function as the honeycomb to induce a pressure drop and to inhibit flow conditions above the diffuser from propagating down into the inflow region. A pressure perturbation above the inlet might propagate into the honeycomb, but the channels would inhibit significant propagation of that disturbance. The simulated inflow condition is consistent with this interpretation of the inflow boundary. Initial simulations omitting the porous region exhibited poor quantitative and qualitative comparisons to the experimental data low in the plume (see Figure A-1). This motivated the porous assumption illustrated in Figure 1 (right). The gas volume fraction was 1.0 at the z-height of 0.0. Below this, the porosity was decreased until a 0.80 gas volume fraction at -0.01 m. Below that, the gas volume fraction was constant.

This inflow condition was arrived at empirically, by examining the predicted planar flow and comparing the contours to experimental results. Note that the coarsest (R4) mesh lacked nodes in the transition region between the maximum and minimum gas volume fraction, so the variation appeared more as a step function for that coarse simulation prediction. The magnitude of the gas volume fraction was the main parameter

adjusted to achieve the final condition used for all the subsequently described simulations (unless otherwise noted). Figure 2 shows a comparison of data and simulation results for the R6 mesh. The most notable variations from the data were in the centerline mass fraction, the vertical velocity at the centerline, and the radial velocity recirculation zones. Contour intervals are all spaced identically in the corresponding images, and the images were manually sized to be approximately similar in scale.

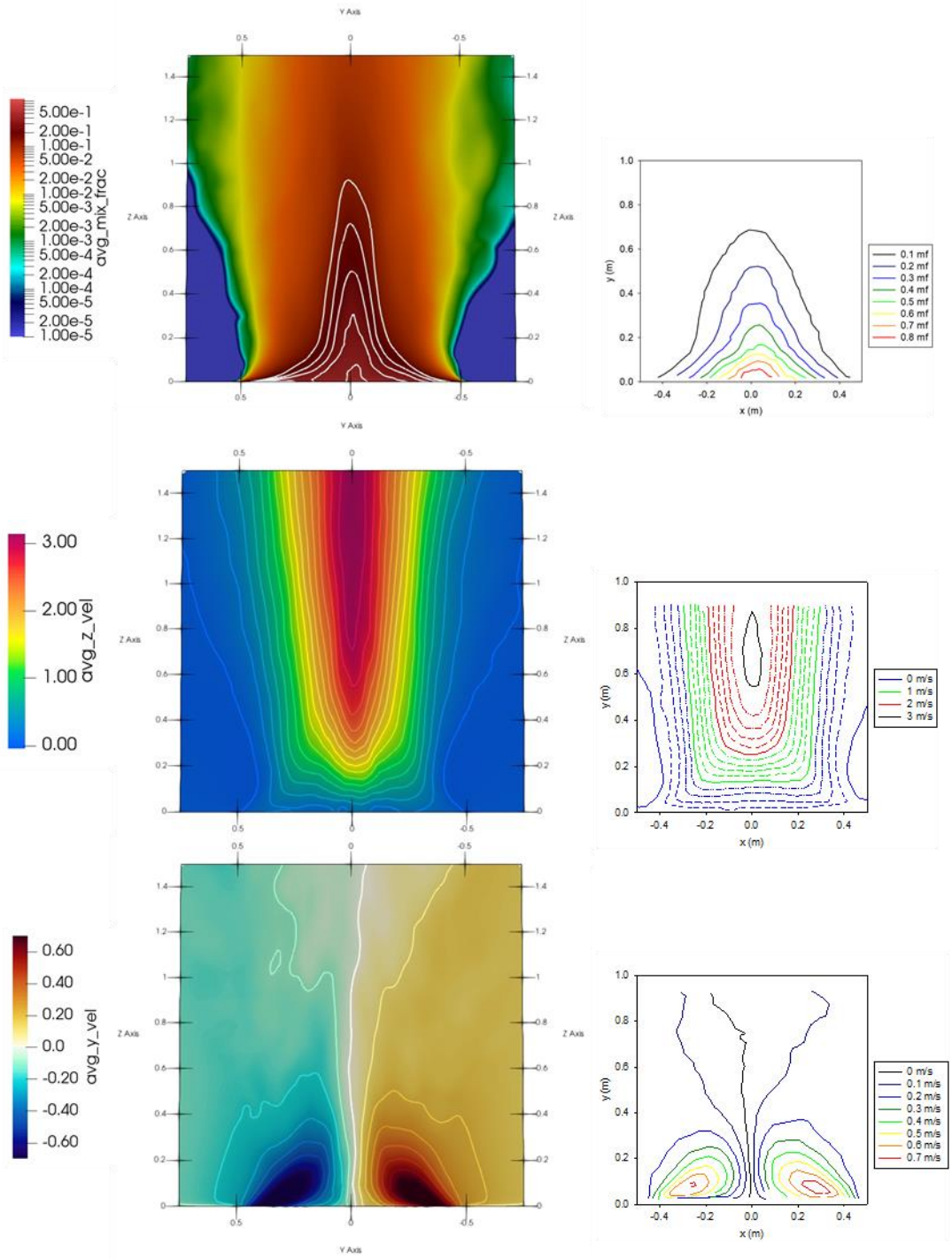

Fig. 2 The R6 simulation results (left) with calibrated inlet compared to the planar data from the tests (right) for mixture fraction (top), vertical velocity (middle), and radial velocity (bottom)

Figure A-1 shows planar images of the variety of assumptions evaluated on the R5 mesh prior to selection of the final simulation inlet conditions. This suggests a moderate to high degree of sensitivity of the results to the inflow boundary condition and helps justify the selected inlet methods.

2.4 Simulation Parameters

The domain selected for this simulation series was a 9 m high, 5.82 m diameter cylindrical mesh, as partially illustrated in Figure 3 (left). This image shows a cut-away of the coarse (R4) mesh. The computational domain is smaller than the full FLAME facility, which presumes that the domain was successful in achieving a semi-infinite condition with respect to the plume. The bottom air inlet was not modeled in favor of a shroud plane simplified air inlet (blue in Figure 3 left) that was functional in the velocity with distance. The lateral extent was inside that of the facility walls as well as the internal cylindrical shroud. The vertical dimension was significantly higher than what might be construed as the facility roof, or the constriction to the exhaust, which was neglected here. The simulations in this way are more representative of an open plume. The effect of the upper structure of the facility on the flow in the measurement region is not well established, but at this point assumed negligible.

Other meshes were used, which included progressive refinement of the baseline mesh. This means that each hexahedral element was split into N equal intervals, where N varied from 0 for the baseline case up to 4 for the finest case run in this effort. A finer mesh existed, but due to resource limitations was not run to completion. Figure 3 (left) shows a graphical representation of the mesh characteristics, while the plot on the right gives the values corresponding to the mesh parameters. Meshes are labelled R4 through R8, with R8 being the finest simulation. Resolution is referenced to the pan region and is characterized by the z- and y-fine dimensions. The z-fine (vertical) value is representative of the length scales of the mesh along the boundary, while the x- and/or y-fine (radial) parameter is more representative of the resolution in the bulk region where data and simulation results are primarily compared. Mesh R4 ran relatively fast, a few days on a few dozen processors. Mesh R8 was challenging to run, requiring a few weeks on around 1000 CPUs.

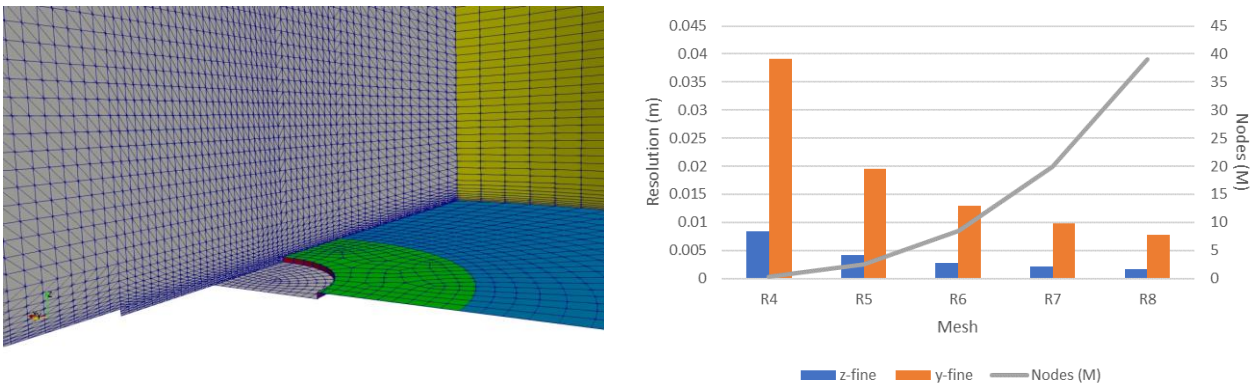

Fig. 3 The R4 coarse mesh (left) and a quantitative illustration of the mesh variations (right) in this study.

2.5 Comparison Methods

It is instructive to make quantitative comparisons between the model and data in addition to the simple plotting of line results. The methods for quantitative comparison are numerous and can give a different picture of the accuracy of the model depending on the chosen approach. Here we elect to illustrate two methods that represent the accuracy of the three main variables and their RMS values. We have previously applied a variety of methods to an even more detailed CFD comparison (see Brown et al., 2021) [7-9]. From that work, the correlation analysis was found to be a preferred metric for comparison. Here we also evaluate the Euclidian norm, a metric proposed by Peacock et al. (1999) [10] for studying model accuracy for fire simulations.

Comparison methods require that the model and experiment be spatially coincident. The intervals of data and model output were different, so this needed rectification. The simulation results are first interpolated onto the data intervals using a linear interpolation. With coincident data, detailed comparisons can be made on each variable. Here the coefficient of determination, or R^2 based on the correlation analysis, is used for assessing model accuracy. The correlation coefficient is calculated as follows:

$$R_{xy} = \frac{\sum_{i=1}^{n}(x_i-\bar{x})(y_i-\bar{y})}{\sqrt{\sum_{i=1}^{n}(x_i-\bar{x})^2}\sqrt{\sum_{i=1}^{n}(y_i-\bar{y})^2}} \quad (1)$$

The correlation analysis is an estimate of the quality of a linear fit between the model and experiment (x and y), which should ideally be linearly related with a slope of 45º.

The Euclidian Norm is also determined for the dataset. This parameter presumes the data and model are in a vector space of n dimensions involving n data points, and that the similarity between the model and data are represented by vector quantities. Vector magnitudes are typically the most interesting component of this analysis. The Euclidian norm E is the distance between the two vectors normalized by the experimental vector magnitude. This gives a sense of the similarity between the model and data in Euclidian terms.

$$E_{xy} = \sqrt{\frac{\sum_{i=1}^{n}(y_i-x_i)^2}{\sum_{i=1}^{n}(y_i)^2}} \quad (2)$$

In this case, the experimental result is the 'y' component. The correlation analysis is different in that it is agnostic to the data source component (i.e., which component is x and which is y).

3. RESULTS

The baseline comparison to the data involved line comparisons for the vertical, and radial velocity and the mass fraction of the helium radially at elevations of 0.2, 0.4, and 0.6 m above the inlet (plots are found in the appendix). RMS values for each variable are also compared. These constitute the baseline MaCFP results and are the context of the additional analysis that is the main subject of this paper.

Figure 4 shows the Euclidian Norm of the predictions for the three variables and their RMS values plotted against the spatial resolution of the finest scales in the simulations (see the right plot of Figure 3 for scale reference versus R# notation). There is a general trend towards improved results as the mesh refinement is increased. All variables should ideally decrease from right to left in this plot. Notably, the vertical or W velocity improves significantly, as does the Y RMS value. In some cases, a refinement results in a worse prediction, like the mass fraction (Y) and radial velocity (U) for the last two steps of refinement. These are generally small, perhaps reflective of the variable having reached a level above which further refinements are unlikely to resolve the data any better. While the direct variables don't always exhibit improvements with refinement, the RMS variables appear to improve significantly with the increased refinement. The Euclidian Norm is best with a value of zero. Prior experience with CFD comparisons using this metric suggest good comparisons are below 0.2 in magnitude, which is achieved for the W-velocity and the U- and W-velocity RMS variables for R8 and some of the other higher resolution meshes.

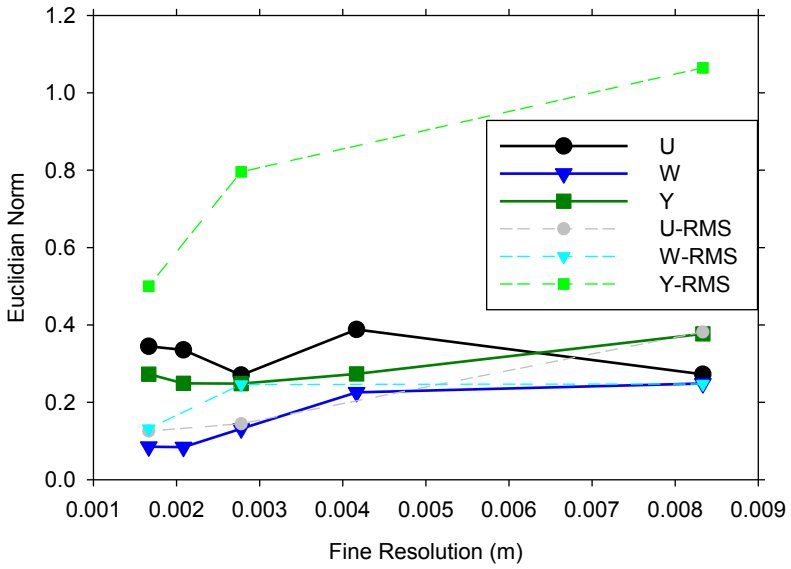

Fig. 4 Euclidian norm for the comparisons as a function of resolution

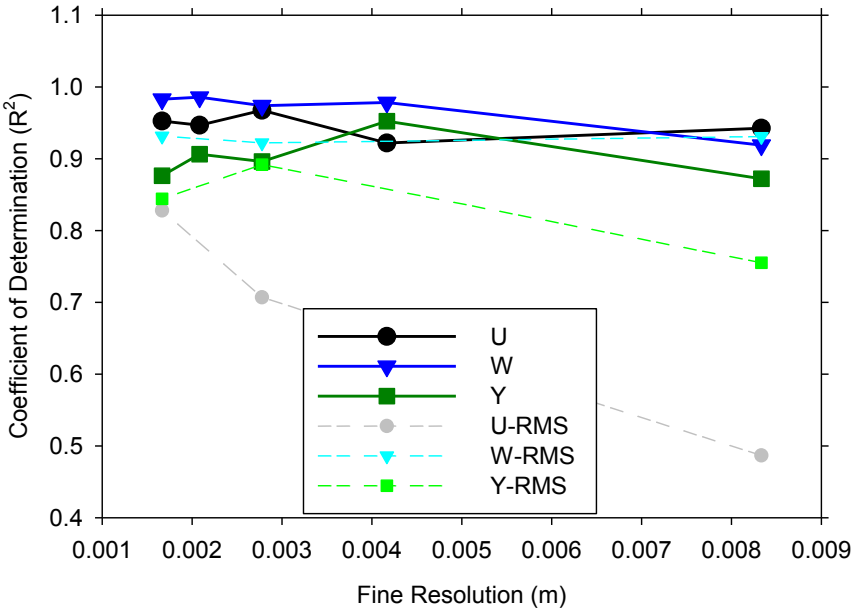

Fig. 5 Coefficient of Determination (R^2) for the comparisons as a function of resolution

Figure 5 shows the coefficient of determination for the primary variables. This parameter has a maximum of 1.0, which is suggestive of a perfect fit. Good fits are in the 0.9 and above range, although prior experience suggests some secondary (gradient) and difficult parameters may be significantly below this value for scenarios with good visual similarity of planar contours. There is a general upward trend moving from right to left in this plot, suggesting improved convergence and improved comparisons with increased resolution. The primary variables do well, although the mass fraction appears to get worse with improved resolution after a point. The U-RMS variable (radial velocity) is particularly poor at the lowest resolution and improves significantly with resolution. The W-RMS variable (vertical velocity) is about as good regardless of resolution. The W-velocity (vertical) comparisons for the highest two resolutions are excellent, approaching the ideal of 1.0.

The radial velocity component is generally much smaller than the vertical, and it seems to contribute greatly to the uncertainty in the system. Looking at the data from a vector angle and magnitude perspective suggests the velocity comparisons are actually quite good, as suggested by Figure 6. Transposed to magnitude, the R^2 values are all above 0.9, and converge towards 1.0. Three angle assumptions were used: A) a straight comparison for all data, B) comparing only where experiment and simulation were above 10% of the maximum velocity, and C) comparing

only where the experimental results were 8% above the maximum. Assumption A suggests poor directional comparison, but after limiting the comparisons to where the velocity was reasonably high (B), the results significantly improve. The C assumption suggests a major increase in the correlation with improved mesh refinement. This suggests that the core of the plume is well predicted by all resolutions both in magnitude and direction. It also suggests that the improved resolution helps better resolve the details of the low average velocity regime to a point. Comparisons are good notwithstanding the questionable application of the method to an angle variable that will wrap around at the 0-360º interface.

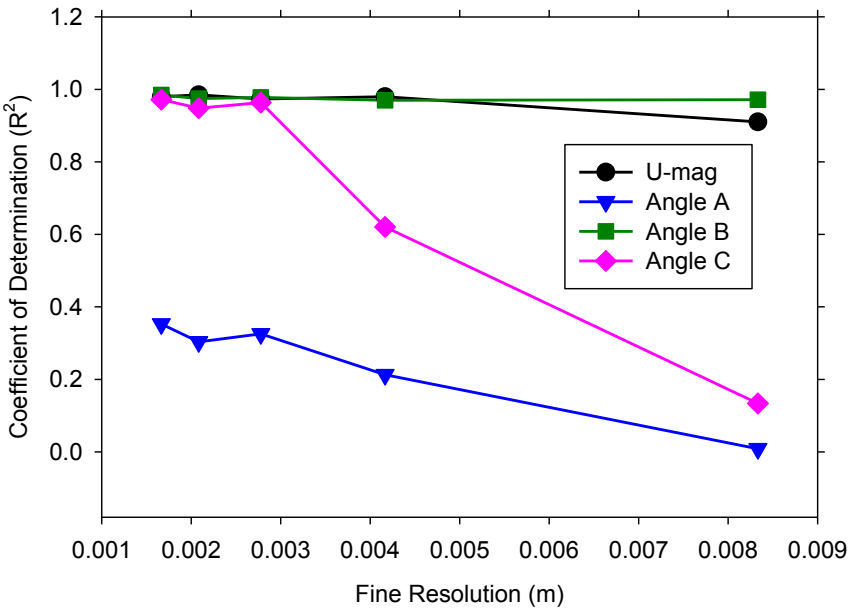

Fig. 6 Coefficient of Determination for the velocity magnitude and angle comparisons as a function of resolution

4. DISCUSSION

The velocity and mass fraction measurement uncertainties are well-described in the journal article presenting the results (O'Hern et al., 2005) [2]. Uncertainties in the velocity means were reported to be ±20% and those for the fluctuations were ±30%. Uncertainties in the mass fraction means were estimated at ±18% plus some systematic offset of ±5%; those in the fluctuations were ±21%. These uncertainties are relatively large because of the challenges associated with measurements in these large-scale flows. The magnitude of these uncertainties can be compared with the Euclidean norms of the differences between measurements and predictions from Figure 4. Where the experimental uncertainties exceed the Euclidean norm differences, it might be reasonable to ascribe agreement between the predictions and measurements. However, a more careful comparison of the profiles as discussed here can provide insight into the prediction trends relative to experimental trends.

In general, referring to Figure 4 and Figure 5, the Euclidian norm and the coefficient of determination for the vertical mean velocity, W, are close enough to their optimal values that we can ascribe good agreement to this quantity for most resolutions, though there is a trend to improve predictions from mesh R5 to R6 and R7. For the vertical velocity profile, it is important to correctly predict both the magnitude of the velocities and the spreading of the plume since the plume spreading is indicative of mass entrainment while the velocity magnitude indicates buoyant acceleration. Considering the profiles in Figure A-2, visual agreement is good for meshes R6, R7 and R8, especially for the 0.4 m and 0.6 m heights. At the lowest height there are small deviations that reflect the challenges in modeling the development of turbulence at the plume base.

The vertical mass flux associated with buoyant plumes, i.e. $\int_0^\infty \pi\rho W r dr$, increases with height. The radial velocity component, U, is important for describing the mean entrainment of the surroundings into the plume that is responsible for this increased mass flux. U-velocity profiles in Figure A-3 appear to have visibly greater differences between the predictions and measurements. However, the U-velocity magnitudes here are almost one order of magnitude smaller so that the absolute differences, on the order of 0.1 m s^{-1} for each of these figures, may be comparable. Of greater concern is the significant differences in the profile shape for the higher heights at 0.4 and 0.6 m and the fact that these differences are enhanced with increasing resolution. It is not clear whether the profile shape differences reflect experimental variability or prediction errors, through there is more right-left asymmetry in these measurements compared to other measurement sources (c.f. Figure A-2 and A-4). The coefficient of determination comparisons suggest good agreement here while the Euclidean norm is generally greater than 0.3, which is larger than expected with the experimental uncertainties of 20%. This larger value for the Euclidian norm might reflect the similar differences (0.1 m s^{-1} for each component mentioned above) normalized by the relatively small magnitude of the entrainment velocities. Also, the analysis of the coefficient of determination in terms of the velocity magnitude and angle from Figure 7 suggests that small differences associated with the components of lower velocity samples significantly influence the comparisons.

The final mean quantity that was measured is the mean plume mass fraction, Y. As noted above in conjunction with Figure A-4, there is a systematic shift from underpredicting the near-center mass fractions at low heights to overpredicting the near-center mass fractions at higher heights, and this shift is amplified as the mesh resolution increases. This occurs despite the radial inflow velocities tending to predict greater values than measured, which would suggest the opposite behavior. It is expected that the integral vertical flux of the plume source, $\int_0^\infty \pi\rho W Y r dr = \pi\rho_0 W_0 D^2/4$, should be conserved, and presumably species/mass conservation within the simulation forces the predictions to maintain a constant vertical flux. One item worth noting is that at the 0.6 m height the measurements suggest that the plume could have spread beyond the measured radii, and this could easily make up for the measured differences. The global measures of prediction accuracy in the Euclidean norm and the coefficient of determination have moderate values for Y, but interestingly the highest resolutions move slightly away from the optimal values. The centerline offset might be ascribed to errors in diffusion or the advective field. The advective field is well predicted and the diffusion is not thought to be so significantly erroneous. It is possible that the use of a mixture fraction to describe the plume gas is culprit. This assumption involves assuming the helium and the acetone (used to generate the experimental signal) were of equal proportion in the inlet and through the lower plume. The degree to which this is not the case may contribute to the centerline errors.

The velocity fluctuations provide the large-scale mixing between the plume and the surrounding. Velocity fluctuations drive the transfer of energy from buoyant vertical acceleration to more random turbulent motions that ultimately lead to viscous and diffusive transport. Because the flow energy is added in the vertical direction, the vertical fluctuation magnitudes are largest, but large coherent vortices are responsible for puffing that transfers the energy between the vertical and horizontal components. The predictions show a trend toward greater transfer of this energy from vertical to horizontal with increasing mesh resolution. This might arise from a greater dynamic range of eddies associated with the transfer. The initial coherent structures need to break down through the turbulent cascade to approach a more isotropic turbulent state. The flow here does not reach a point where velocity fluctuations are isotropic, and this is a part of the reason that large-eddy simulations perform significantly better for buoyant plumes than Reynolds-averaged simulations (which were not the direct subject of this study). The Reynolds-averaged Navier-Stokes (RANS) simulations are generally implemented with an assumption of isotropic velocity fluctuations, at least when solving for a single turbulent kinetic energy instead of the full Reynolds stress tensor. All comparison metrics suggest the velocity fluctuations are better predicted with higher mesh resolution.

The mass-fraction fluctuations presented in Figure A-7 show the predictions as having uniformly greater fluctuations than the measurements with a magnitude that exceeds the expected measurement uncertainties. Scalar fluctuations like this are relevant to the overall scalar transport through terms that (in RANS) would be of the form $\overline{U'Y'}$. While the correlation is a part of this quantity, overpredictions of the scalar fluctuations would be expected to lead to predictions of faster plume spreading in terms of the scalar profiles in Figure A-4. Faster spreading of the mean mass fraction is not generally observed in these figures, so it is difficult to interpret the significance of the overprediction shown in the fluctuations. Scalar fluctuations in fires can be important measures of

unmixedness, suggesting slower fuel-air mixing. If this is an issue it might be reflected in higher flame heights as fuel pockets mix with air more gradually in predictions. This can be assessed in separate flame height comparisons. For fires in enclosures, flame height can be less of an issue, but the mixing of the plume with its surroundings is an important factor in assessing hazards associated with light and buoyant gas releases.

In terms of resolution requirements for accurate simulation, it is seen that there are diminishing improvements for R6 and above, while resolution R4 through R6 show marked improvements with added resolution. This lends to the notion that plume mixing with CFD can be linked to the radial resolution, and that around 80 elements across a diameter is necessary to achieve nearly resolved advective mixing (as per R6). Further refinements exhibit the most benefit for some RMS parameters, but have lesser effects on the direct variables in these comparisons.

6. CONCLUSIONS

This paper presents a unique analysis of a turbulent buoyant plume predicted with CFD. Comparisons are made for a variety of uniformly refined mesh resolutions for scalar and RMS velocity and mass fractions. The Euclidian norm and the coefficient of determination (R^2) give generally similar trends exhibiting the improvement of accuracy with resolution. Differences exist in the relative magnitude of error for some components. RMS predictions improve the most with increased resolution. Transforming the radial and vertical velocities to magnitude and direction indicates the magnitude of velocity is well predicted, and the direction is well predicted except where velocity magnitudes are low. Mass fraction is less well predicted, possibly attributable to the mass fraction modeling assumption and differential diffusion. RMS predictions improve the most with added resolution, and somewhere around 80 elements across a diameter (the R6 scenario) which seems to result in converging flow simulation results.

ACKNOWLEDGMENT

Sandia National Laboratories is a multimission laboratory managed and operated by National Technology and Engineering Solutions of Sandia, LLC., a wholly owned subsidiary of Honeywell International, Inc., for the U.S. Department of Energy's National Nuclear Security Administration under contract DE-NA-0003525. This paper describes objective technical results and analysis. Any subjective views or opinions that might be expressed in the paper do not necessarily represent the views of the U.S. Department of Energy or the United States Government.

REFERENCES

[1] Brown, A., Bruns, M., Gollner, M., Hewson, J., Maragkos, G., Marshall, A., McDermott, R., Merci, B., Rogaume, T., Stoliarov, S. and Torero, J., 2018. Proceedings of the first workshop organized by the IAFSS Working Group on Measurement and Computation of Fire Phenomena (MaCFP). *Fire safety journal*, 101, pp.1-17.

[2] O'Hern, T.J., Weckman, E.J., Gerhart, A.L., Tieszen, S.R. and Schefer, R.W., 2005. Experimental study of a turbulent buoyant helium plume. *Journal of Fluid Mechanics*, 544, p.143.

[3] Blanchat, T.K., "Characterization of the Air Source and the Plume Source at FLAME," Sandia Report SAND 2001-2227.

[4] Sierra Thermal Fluids Development Team, "Sierra Low Mach Module: Fuego Theory Manual – Version 4.44," Sandia National Laboratories, SAND 2017-3774, (2017).

[5] Sierra Thermal Fluids Development Team, "Sierra Low Mach Module: Fuego User Manual – Version 4.44," Sandia National Laboratories, SAND 2017-3792, (2017).

[6] Kerstein, A.R., M.A. Cremer, and P.A. McMurtry, Scaling Properties of Differential Molecular Diffusion Effects in Turbulence. *Phys. Fluids*, 7(8):1999-2007 (1995)

[7] Brown, A.L., Clemenson, M.D., Benson, M., Elkins, C. and Jones, S.T., 2021. An urban dispersion inspired scenario for CFD model validation. *Fire Safety Journal*, 120, p.103130.

[8] Brown, A.L., Lance, B.W., Clemenson, M., Jones, S.T., Benson, M., Elkins, C., "Dispersion Validation for Flow Involving a Large Structure Revisited: 45 Degree Rotation," SAND2020-10124

[9] Brown, A.L., Benavidez, E. "Dispersion Validation for Flow Involving a Large Structure," SAND2018-9380, August 2018

[10] Peacock, R.D., Reneke, P.A., Davis, W.D. and Jones, W.W., 1999. Quantifying fire model evaluation using functional analysis. *Fire Safety Journal*, 33(3), pp.167-184.

APPENDIX

Figure A-1 shows predictions with a variety of inlet assumption and helps justify the final selection of the inlet configuration for these simulations.

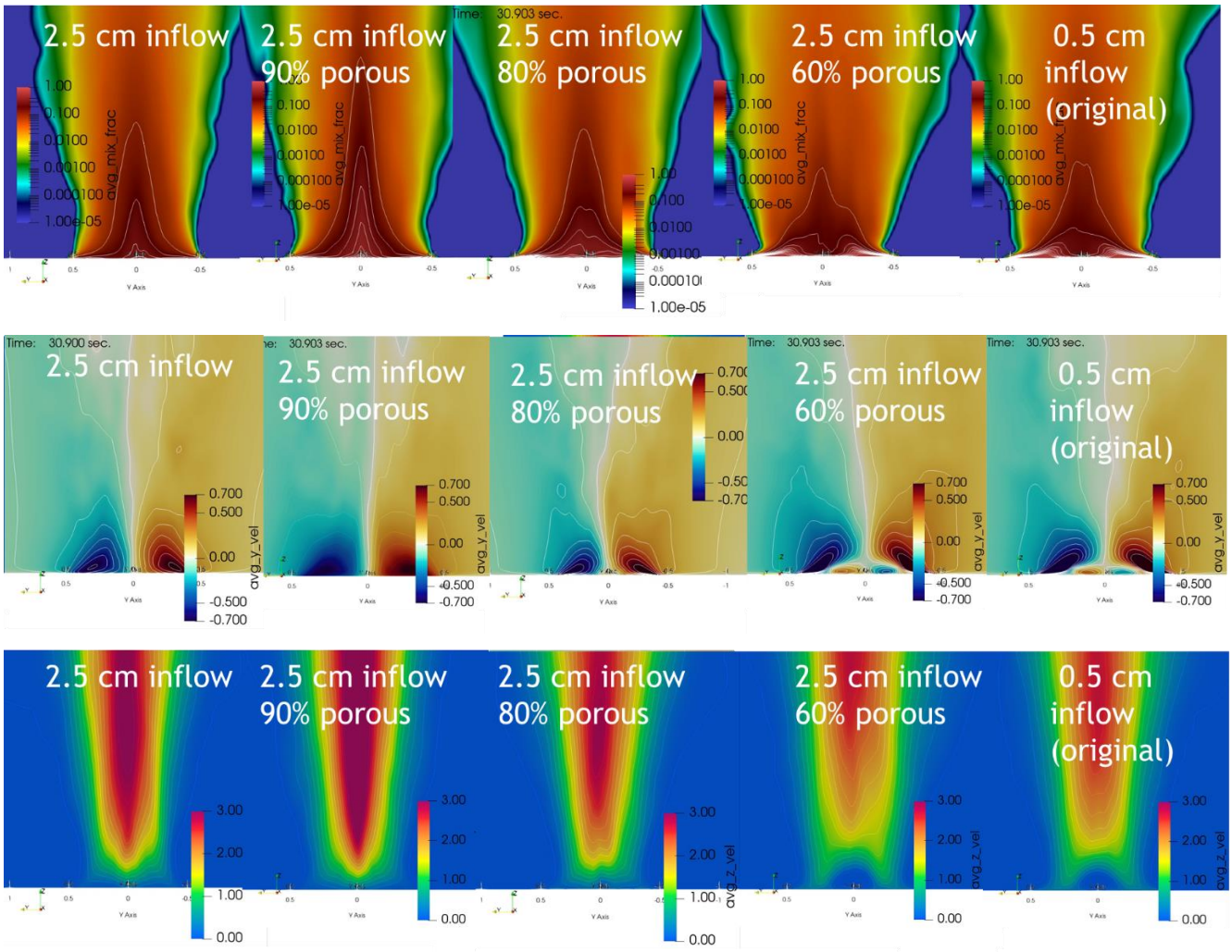

Fig. A-1 The R5 planar results with a variety of inlet assumptions for mixture fraction (top), radial velocity (middle), and vertical velocity (bottom)

The vertical component of velocity here is termed the W velocity, and involves the highest magnitude velocities from the test, as motion is primarily vertical. Figure A-2 shows predictions at 0.2, 0.4, and 0.6 m heights. There is an obvious improvement in the results, with R4 predictions clearly deviating from the data, and the progressive refinement results showing trending towards the data. The highest level of refinement (R8) gives a very good approximation of the data and are with few exceptions trending with the data. 0.2 m elevation results are in the upper-left, 0.4 m results in the upper-right, and 0.6 m results in the bottom-left. This convention is held for all subsequent plots.

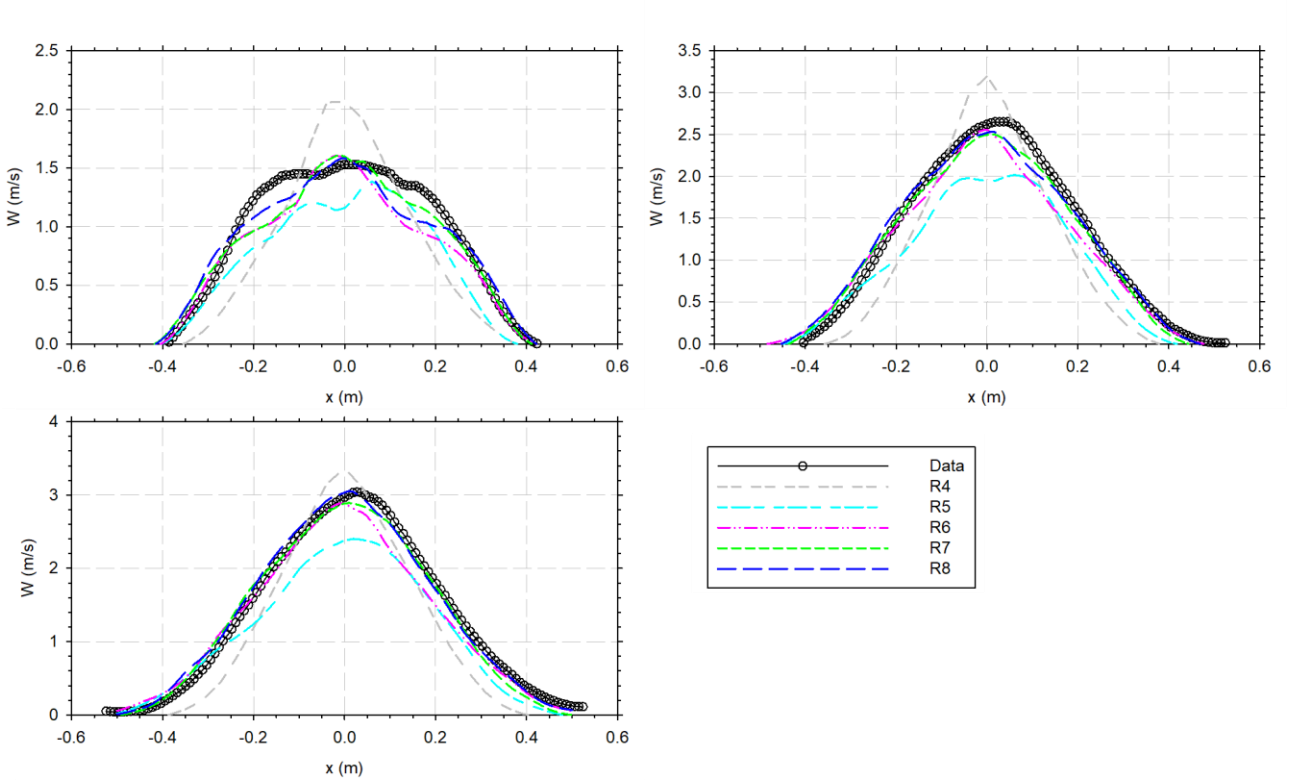

Fig. A-2 Vertical velocity comparisons with data

The radial component of the velocity is the U-velocity, and results are shown in Figure A-3. It is important to keep in mind that the geometry is ostensibly symmetric, and the data and models should exhibit corresponding behavior. For the most part, the models do this well, however a moderately large example of the data lacking symmetry is found in the data in Figure A-3 where +/- 0.4 m data differ significantly. Major trends are well predicted. However, inflection points tend to be different between the models and data.

Note the difference in the magnitude of the U-velocity compared with the figures in the prior section. The magnitude of velocity is about an order of magnitude higher for the vertical velocity. Were these plotted on a similar scale, the U-velocity comparisons might appear much more accurate when compared with the data.

Figure A-4 shows mass fraction comparisons. The data tend to be higher than the models at low (0.2 m) levels, and pretty accurate at intermediate heights (0.4 m). At the highest elevation, data tend lower than the model. This elevation bias is somewhat surprising, as there is not a similar velocity offset that would tend to suggest an advective source for the differences. Further, the radial entrainment velocity predictions in the previous set of Figure A-4 generally suggests greater entrainment in the predictions. We expect this would tend to increase the dilution and spreading of the plume mass fraction more than in the measurements, but the opposite appears in this set of figures. This might be suggestive of some diffusional bias, but it could have its source in other variabilities. Note also that the peak data are slightly skewed in the positive-x direction, whereas the model predictions tend to be symmetric. The breadth of the peaks is reasonably predicted, which suggests the effect causing the discrepancy is center-line dominant.

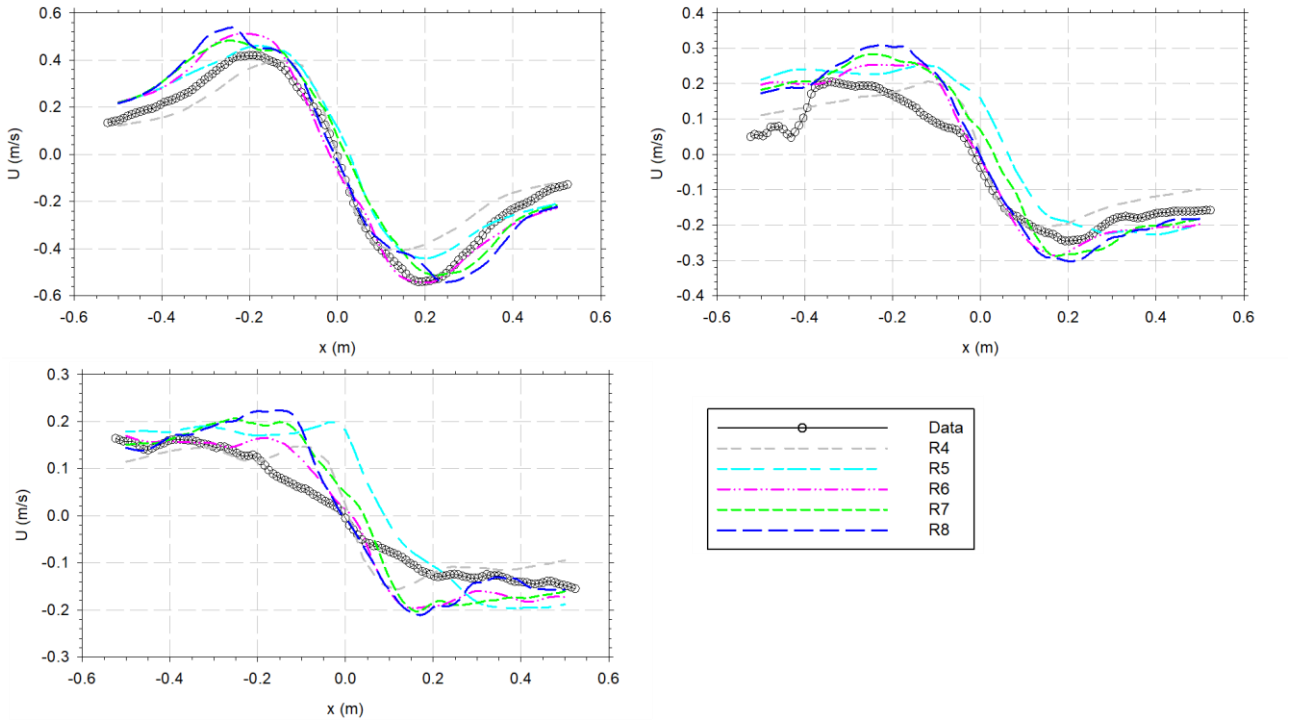

Fig. A-3 Radial velocity comparisons with data

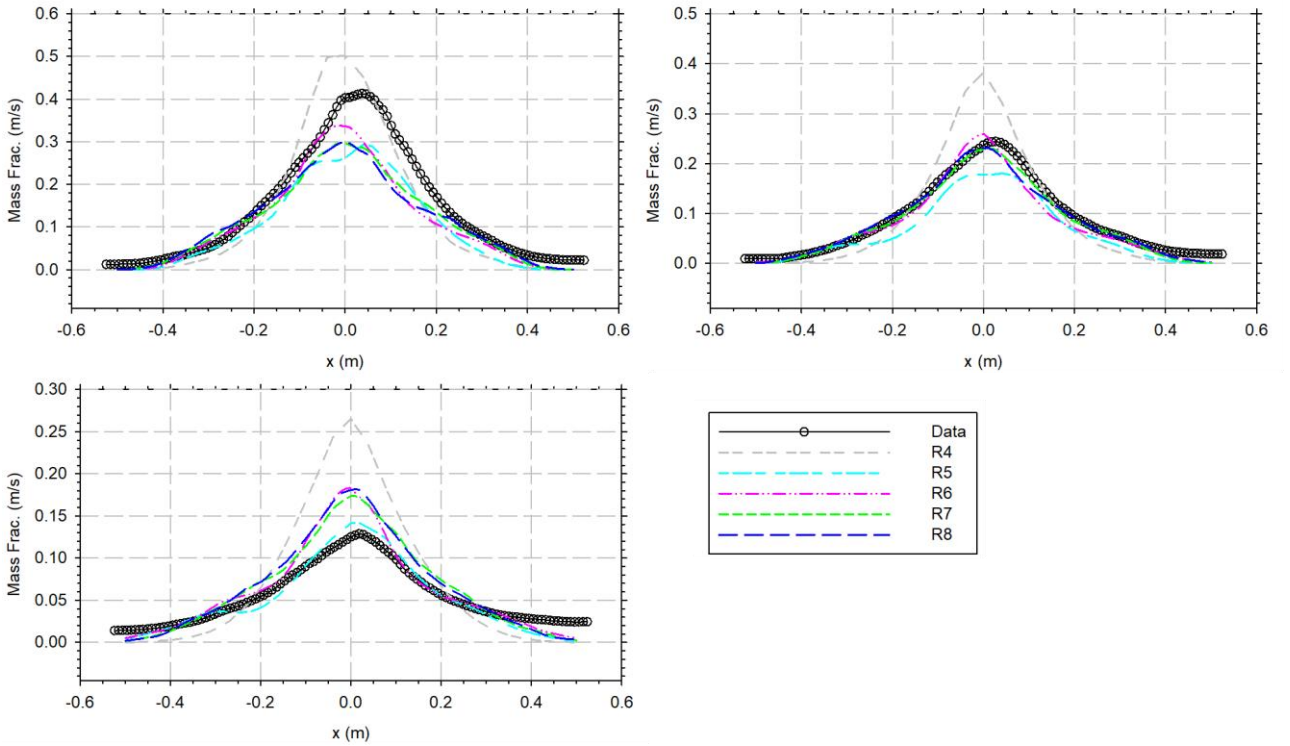

Fig. A-4 Mass fraction comparisons with data

Root-mean-squared (RMS) fluctuating velocity was also provide by the tests and was extracted from the model predictions at three of the mesh resolutions. These were extracted based on 300-400 instances of the developed plume results, and post-processed from the domain extractions for the R4, R6, and R8 meshes. The RMS is also equal to the standard deviation (STD) of the velocity. Figure A-5 shows vertical velocity (W-velocity) at 0.2, 0.4,

and 0.6 m elevation RMS predictions versus the data. In each case, there is a clear improvement of the model predictions from R4 to R8 in terms of the shape of the trends and the peak magnitudes. This provides evidence of improving predictions of the dynamic behavior of the plume as mesh resolution increases.

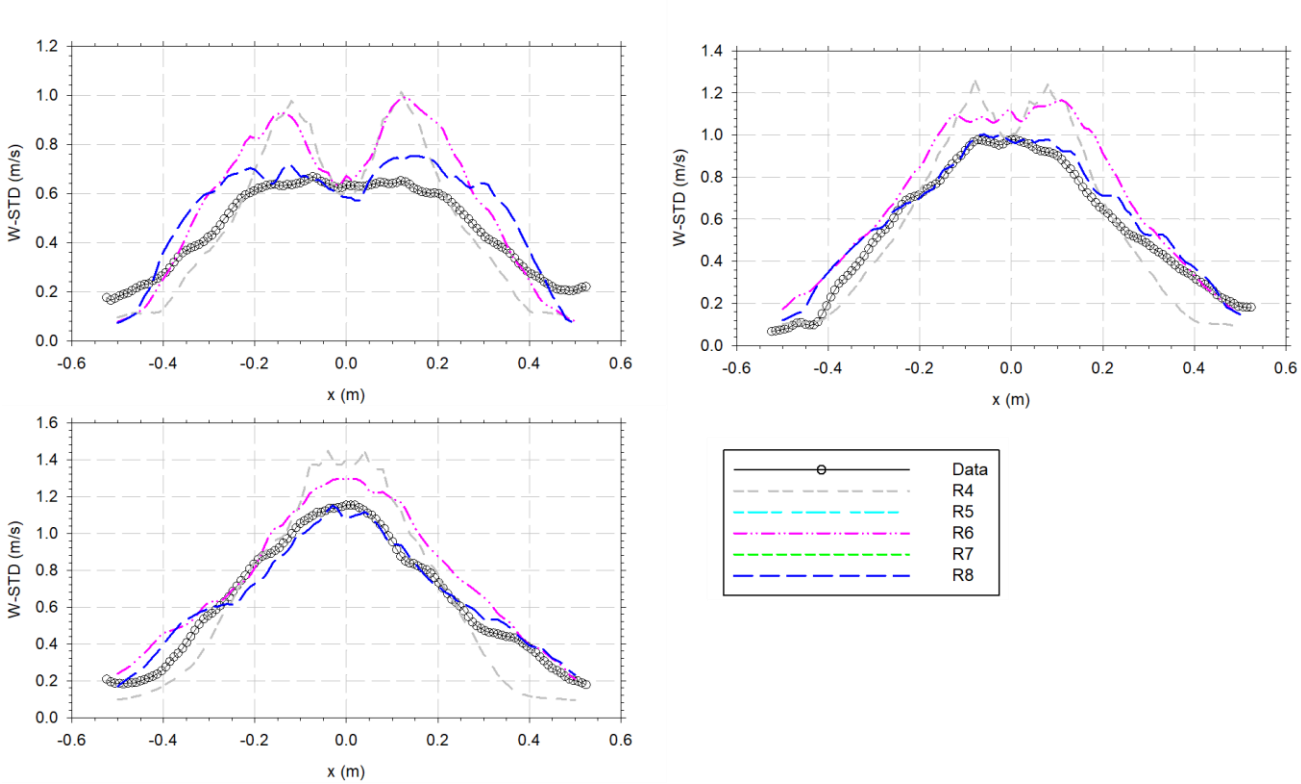

Fig. A-5 Vertical Velocity RMS comparisons with data

Figure A-6 shows U-Velocity RMS comparisons for the three simulations versus the data. In all cases, the R4 simulations are clearly poorer than the others compared to the data. The R6 and R8 simulations resolutions do much better and are mostly indistinguishable except at 0.2 m where R6 curiously appears better than R8. Note here as with the magnitude plots that the fluctuations in the radial velocity are much smaller in magnitude than the corresponding vertical velocity fluctuations. We note that increased resolution tends to lead to greater radial U-velocity fluctuations while increased resolution tends toward lower vertical W-velocity fluctuations. This suggests that increased isotropy in the turbulent kinetic energy results from resolution, or perhaps that the anisotropy associated with acceleration tends to remain in the vertical component when there is less resolution and less of a turbulent cascade.

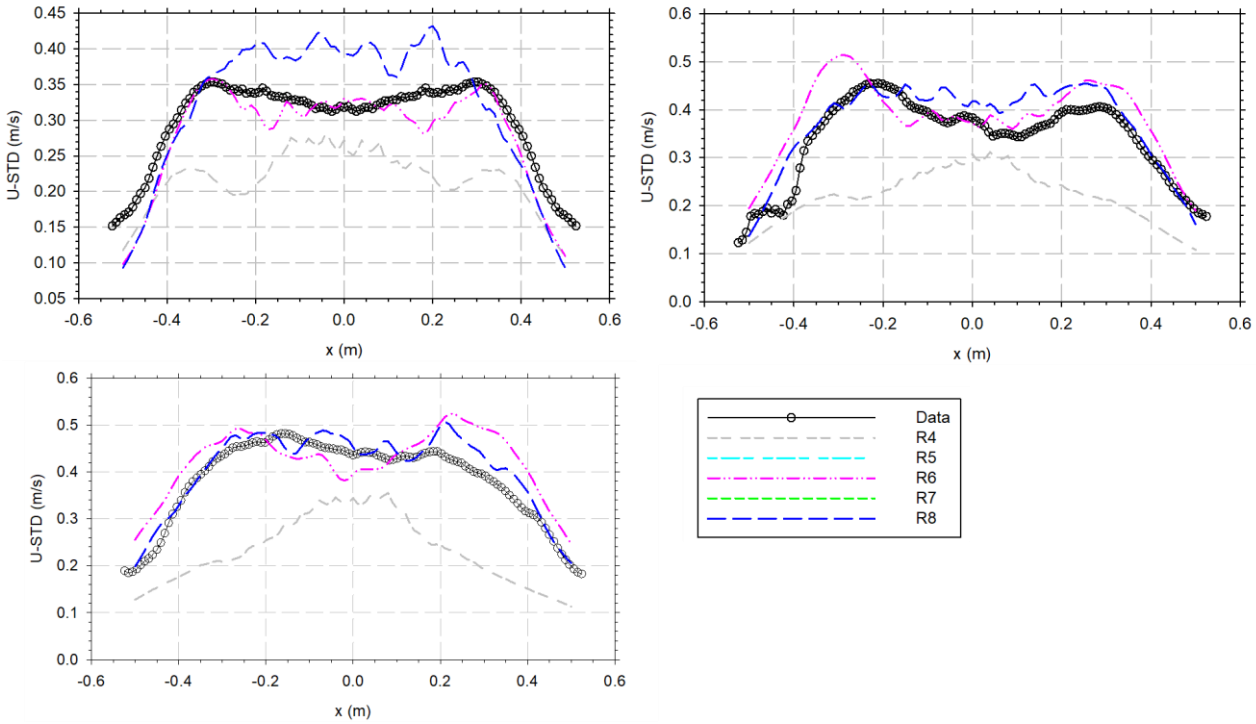

Fig. A-6 Radial Velocity RMS comparisons with data

Figure A-7 shows the mass fraction RMS predictions compared with data. The simulations generally predict higher fluctuations than the data, and trending is good for the R6 and R8 mesh resolutions. Like the scalar data for mass fraction, there is an asymmetric skew to the RMS data that do not appear in the model predictions. It is curious that the mass fraction RMS is moderately lower than predictions given that the predicted velocity fluctuations were a reasonable approximation of the data. This would seem to point to a diffusive error rather than an advective error, since the velocity fluctuations appear to converge towards the data.

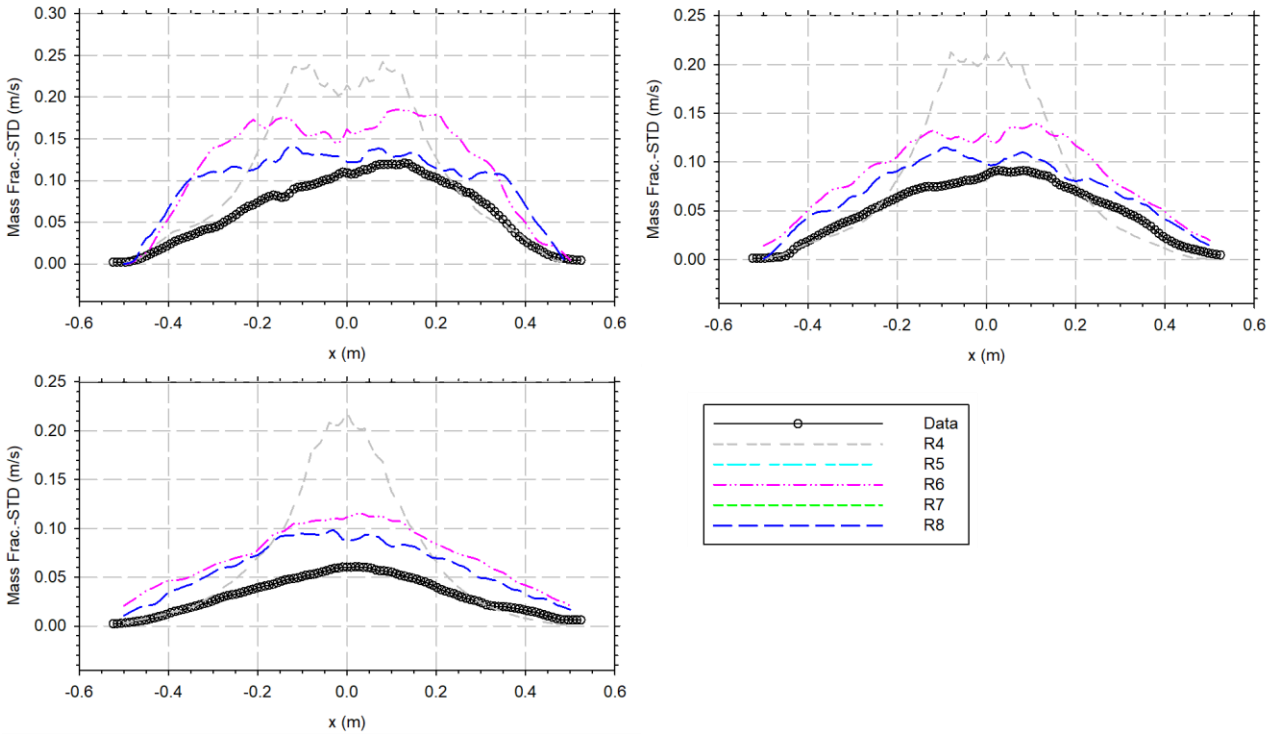

Fig. A-7 Mass fraction RMS comparisons with data